View metadata, citation and similar papers at core.ac.uk
brought to you by CORE
provided by Elsevier - Publisher Connector

Biochimica et Biophysica Acta 1808 (2011) 1832–1842

Contents lists available at ScienceDirect

Biochimica et Biophysica Acta

journal homepage: www.elsevier.com/locate/bbamem

Comparative study of clinical pulmonary surfactants using atomic force microscopy

Hong Zhang [a,b], Qihui Fan [a], Yi E. Wang [a], Charles R. Neal [c], Yi Y. Zuo [a,*]

[a] Department of Mechanical Engineering, University of Hawaii at Manoa, Honolulu, HI 96822, USA
[b] Department of Respiratory Medicine, Peking University First Hospital, Beijing 100034, China
[c] Department of Pediatrics, John A. Burns School of Medicine, University of Hawaii, Honolulu, HI 96826, USA

ARTICLE INFO

Article history:
Received 23 December 2010
Received in revised form 21 February 2011
Accepted 14 March 2011
Available online 23 March 2011

Keywords:
Surfactant replacement therapy
Dipalmitoyl phosphatidylcholine
Cholesterol
Domain formation
Surface tension
Monolayer

ABSTRACT

Clinical pulmonary surfactant is routinely used to treat premature newborns with respiratory distress syndrome, and has shown great potential in alleviating a number of neonatal and adult respiratory diseases. Despite extensive study of chemical composition, surface activity, and clinical performance of various surfactant preparations, a direct comparison of surfactant films is still lacking. In this study, we use atomic force microscopy to characterize and compare four animal-derived clinical surfactants currently used throughout the world, i.e., Survanta, Curosurf, Infasurf and BLES. These modified-natural surfactants are further compared to dipalmitoyl phosphatidylcholine (DPPC), a synthetic model surfactant of DPPC:palmitoyl-oleoyl phosphatidylglycerol (POPG) (7:3), and endogenous bovine natural surfactant. Atomic force microscopy reveals significant differences in the lateral structure and molecular organization of these surfactant preparations. These differences are discussed in terms of DPPC and cholesterol contents. We conclude that all animal-derived clinical surfactants assume a similar structure of multilayers of fluid phospholipids closely attached to an interfacial monolayer enriched in DPPC, at physiologically relevant surface pressures. This study provides the first comprehensive survey of the lateral structure of clinical surfactants at various surface pressures. It may have clinical implications on future application and development of surfactant preparations.

© 2011 Elsevier B.V. All rights reserved.

1. Introduction

The use of clinical pulmonary surfactant began three decades ago since Fujiwara et al. first reported a successful trial of surfactant therapy in a small group of premature infants using a modified natural surfactant extracted from bovine lungs [1]. Since then, surfactant replacement therapy has become the standard therapeutic intervention to treat respiratory distress syndrome (RDS) in preterm infants [2]. With its use over the past three decades, it is estimated that surfactant therapy alone contributes to a 6% reduction in infant mortality in the United States [3].

A number of clinical surfactant preparations have been developed worldwide. Based on the surfactant protein content, these preparations are generally divided into the first-generation protein-free synthetic surfactants, the new generation synthetic surfactants that contain simplified peptides or recombinant surfactant protein analogs, and the modified natural surfactants derived from animal sources [3–5]. Among these preparations, protein-free synthetic surfactants have faded away partly due to their relatively poor biophysical properties but more because of suboptimal clinical performance; while peptide-containing synthetic surfactants, although promising, are still under development [3].

Being the only surfactant preparations used in current clinical practice, animal-derived modified-natural surfactants have been extensively studied. Meta-analyses and retrospective reviews on the comparison between modified-natural surfactants and synthetic surfactants [6–10], comparison among different modified-natural surfactants [11,12], and comparison of surfactant administration regimes [13,14], are well documented. Compared to the systematic study of these surfactant preparations in clinical trials, there are few *in vitro* studies that compare their biochemical and biophysical properties [15–17]. Direct characterization and comparison of surfactant films at the microscale and nanoscale are still lacking.

Application of microscopic and surface spectroscopic techniques to the study of pulmonary surfactants has revolutionized our understanding of these preparations in the last decade [5,18,19]. Direct film imaging with fluorescence microscopy, scanning probe microscopy, and time-of-flight secondary ion mass spectrometry (ToF-SIMS) has revealed phospholipid phase separation, phospholipid–protein interaction, and localized chemical composition of pulmonary surfactant films [5,18,19]. This information significantly complements the conventional *in vitro* assessment of clinical surfactants, and is especially crucial for mechanistic study.

Among the different biophysicochemical characterization techniques, atomic force microscopy (AFM) has been proven to be an ideal imaging technique and sensitive probing tool for studying pulmonary surfactant films [5,18–21]. AFM is superior to conventional fluorescence microscopy by permitting submicron resolution and eliminating the

* Corresponding author at: 2540 Dole St, Holmes Hall 302, Honolulu, HI 96822, USA. Tel.: +1 808 956 9650; fax: +1 808 956 2373.
E-mail address: yzuo@hawaii.edu (Y.Y. Zuo).

0005-2736/$ – see front matter © 2011 Elsevier B.V. All rights reserved.
doi:10.1016/j.bbamem.2011.03.006

use of fluorescence dyes. It also requires no staining procedure, which is requisite in electron microscopy. Moreover, AFM can detect not only two-dimensional but also three-dimensional topographic features and hence is capable of studying both monolayered and multilayered surfactant films.

In the present study, we report the first comprehensive comparison of film structure for all major animal-derived clinical surfactants currently used throughout the world, including Survanta (Abbott Laboratories, North Chicago, IL, USA), Curosurf (Chiesi Farmaceutici, Parma, Italy), Infasurf (ONY Inc., Amherst, NY, USA), and BLES (BLES Biochemicals, London, ON, Canada). Survanta and Infasurf are licensed in the USA. Survanta is also licensed in Japan under the trade name of Surfacten (Tokyo Tanabe, Tokyo, Japan). Curosurf is licensed in Europe and the USA (Cornerstone Therapeutics, Cary, NC, USA). BLES is licensed mainly in Canada. To gain a better understanding of the surfactant composition–structure correlation, we also include in the comparison pure dipalmitoyl phosphatidylcholine (DPPC), DPPC:palmitoyl-oleoyl phosphatidylglycerol (POPG) (7:3) as a simple protein-free model system, and endogenous bovine natural surfactant (BNS) without organic extraction to preserve the actual *in vivo* surfactant compositions, including surfactant protein A (SP-A).

2. Materials and methods

2.1. Materials

DPPC (16:0/16:0 PC) and POPG (16:0/18:1 PG) were purchased from Avanti Polar Lipids (Alabaster, AL, USA) and used without further purification. Both DPPC and POPG were dissolved in chloroform to form stock solutions at 1 mg/mL. A simple protein-free model surfactant was prepared by mixing DPPC and POPG at a weight ratio of 7 to 3. In spite of being a very simple model system, DPPC:POPG (7:3) contains both zwitterionic (PC) and anionic (PG) headgroups, and both disaturated (dipalmitoyl) and unsaturated (palmitoyl-oleoyl) acyl chains. It has been proven to be a simple yet effective model to represent some biophysical properties of natural surfactants [5].

Bovine natural surfactant (BNS) was obtained from bronchopulmonary lavage of freshly slaughtered cattle with a saline/magnesium chloride/calcium chloride solution and isolated by density gradient centrifugation [22]. Without organic extraction, BNS preserves most components of the endogenous surfactant, including the hydrophilic SP-A. The phospholipid concentration of the original stock suspension was determined to be ~16 mg/mL by the phosphorus assay. BNS was stored frozen. At the day of experiment it was diluted to 5 mg phospholipids/mL using a saline buffer of 0.9% NaCl, 1.5 mM $CaCl_2$, and 2.5 mM HEPES, adjusted to pH 7.0.

Curosurf, Infasurf, and BLES were donated by the pharmaceutical companies and Survanta was obtained from the Newborn Special Care Unit at Kapi'olani Medical Center for Women and Children. These clinical preparations are designated modified-natural surfactants as they undergo organic extraction during the manufacture, which removes the hydrophilic protein (SP-A) and in some cases reduces the content of hydrophobic proteins (SP-B/C) [15]. Additional procedures are involved in the manufacture of Survanta, Curosurf and BLES to remove/reduce neutral lipids, mainly cholesterol. Survanta is further supplemented with synthetic DPPC, palmitic acid and tripalmitin. The detailed chemical compositions of these four clinical surfactants have been well-documented [4,5,15–17,22–24] and summarized in Table 1 together with synthetic surfactants and BNS, in the order of approximately decreasing DPPC content. It should be noted that these values are obtained from the manufacturers and from the literature, and because in some cases different methodologies have been applied, direct comparison cannot necessarily be made in all cases. All four clinical surfactants were extracted by chloroform-methanol using a method modified from Bligh and Dyer [25]. The chloroform-methanol extracts were dried under a nitrogen stream and re-dissolved in chloroform to a final concentration of 1 mg/mL. All stock solutions were stored at −20 °C until use.

All solvents used were HPLC grade. The water used was Milli-Q ultrapure water (Millipore, Billerica, MA) which has a resistivity higher than 18 MΩ-cm at room temperature.

2.2. Methods

2.2.1. Langmuir–Blodgett trough

Spreading, compression and Langmuir–Blodgett (LB) transfer of surfactant films were conducted with a LB trough (KSV Nima, Coventry, UK) at room temperature (20 ± 1 °C). This trough is equipped with two Delrin barriers to minimize film leakage [26]. The trough contains a ~160 mL subphase and has a large operational surface area of ~300 cm^2, which overcomes the pressure restriction imposed by a smaller trough [20,21].

2.2.1.1. Film spreading. All films were prepared by spreading samples on ultrapure water. Our previous studies showed that spreading on buffer instead of pure water caused no detectable differences in the compression isotherms [20,21]. Films were spread by depositing tiny droplets of samples uniformly throughout the air–water interface using a 10 μL microsyringe. Synthetic (DPPC and DPPC:POPG) and clinical surfactant preparations (Survanta, Curosurf, Infasurf and BLES) were spread from 1 mg/mL chloroform-extracted solutions, while BNS was spread from a 5 mg/mL aqueous suspension. Our previous studies have demonstrated that spreading a clinical surfactant (BLES) from a chloroform-extracted solution or an aqueous suspension dose not affect the compression isotherm and film structure [20,21]. All initial spreading increased surface pressure (π) to 1–3 mN/m. The volume of spread samples varies from 20 to 30 μL for different surfactant preparations. After spreading, all films were left undisturbed for 10 min to allow equilibrium and evaporation of solvent.

2.2.1.2. Film compression. All spread films were compressed at a rate of 20 cm^2/min, namely 0.1% initial surface area per second. During compression, surface pressure–area (π–A) isotherms were recorded. The trough surface area (cm^2) rather than the absolute molecular area ($Å^2$/molecule) was used to express the compression isotherms. This is due to the difficulty of controlling the exact amount of surfactant molecules at the air–water interface (thus the accurate molecular area) when the films were spread from aqueous media (as to BNS) [20,21], and the difficulty of actually estimating the molecular mass of different clinical surfactant preparations (as to Survanta, Curosurf, Infasurf and BLES). The use of surface area also facilitates the comparison of compression isotherms of different surfactant preparations.

2.2.1.3. Film transfer. For atomic force microscopy imaging, surfactant films at the air–water interface were transferred to the surface of freshly cleaved mica using the LB technique. Surfactant films at controlled constant π were deposited onto the mica surface by elevating the previously submerged mica vertically through the air–water interface at a rate of 1 mm/min. Deposited films were scanned by AFM within 2 hours of deposition. Aging of LB films in air over this time period is considered to have negligible effects on film structure [20,21].

2.2.2. Atomic force microscopy (AFM)

Topographical images of LB samples were obtained using an Innova AFM (Bruker, Santa Barbara, CA). Samples were scanned in air. Each sample was characterized at multiple locations with various scan areas to ensure the detection of representative structures. Both contact mode and tapping mode were used. The different scan modes gave equivalent results. A silicon nitride cantilever with a spring constant of 0.12 N/m and a nominal tip radius of 2 nm was used in contact mode, and a silicon probe with a resonance frequency of 300 kHz and a spring constant of 40 N/m was used in tapping mode. Scan parameters, such as the

Table 1
Lipid and protein compositions of synthetic, modified-natural, and natural surfactants used in this study [4,5,15–17,22–24].[a]

Generic name	DPPC	DPPC:POPG(7:3)	Beractant	Poractant alfa	Calfactant	BLES	BNS
Trade name	–	–	SURVANTA®	CUROSURF®	INFASURF®	BLES®	–
Source	Synthetic	Synthetic	Bovine lung mince	Porcine lung mince	Calf lung lavage	Bovine lung lavage	Bovine lung lavage
Phospholipids	100	100	84	99	91	96	85
PC/DPPC	100/100	70/70	71/50	69/47	79/43	77/41	69/36
PG	0	30	2.4	1.2	4.5	13	10
PE	0	0	3.4	4.5–7.4	2.8	2.6	3.0
PI + PS	0	0	1.3	4.5–8.4	4.0	1.0	2.0
LPC	0	0	1.5	1.0–7.0	< 1.0	0.9	0.2
SM	0	0	3.4	1.8–7.9	0.8	1.4	2.0
Neutral Lipids							
Cholesterol	0	0	< 0.2	0	5–8	2–3	5–8
Free fatty acids	0	0	5.8–14	n/a	0.64	n/a	0.25
Hydrophilic Proteins (SP-A)	0	0	0	0	0	0	8.0
Hydrophobic proteins	0	0	0.94	1.1	1.6–2.2	2.0	2.0
SP-B	0	0	0.04	0.4	0.9	0.5	1.0
SP-C	0	0	0.9	0.7	0.7–1.3	1.5	1.0

BLES: Bovine lipid extract surfactant; BNS: bovine natural surfactant; PC: phosphatidylcholine; DPPC: dipalmitoyl phosphatidylcholine; POPG: palmitoyl-oleoyl phosphatidylglycerol; PG: phosphatidylglycerol; PS: phosphatidylserine; PE: phosphatidylethanol; PI: phosphatidylinositol; LPC: lysophosphatidylcholine; SM: Sphingomyelin; SP: surfactant protein.
[a] Data shown in this table represent weight percentage of each composition with respect to the total mass of pulmonary surfactant.

deflection setpoint, proportional–integral–derivative (PID) gains, and scan rate, were optimized in such a way that the lowest force and highest gains possible were used to scan the sample [27]. Analysis of the AFM images, such as determination of relative height of the surface topography, was carried out by Nanoscope software (ver. 7.30). ImageJ (National Institutes of Health, Bethesda, MD) was used to quantify area fractions of condensed domains.

2.2.3. Statistics

For each surfactant, LB sample preparation was repeated for at least 3 times at each surface pressure. Multiple AFM images were taken for each sample at each surface pressure. All data are expressed as mean ± SD (n > 5 unless otherwise indicated). Group differences were analyzed by one-way ANOVA using OriginPro8.0. A $P < 0.05$ was considered statistically significant.

3. Results

3.1. Comparison of compression isotherms

Fig. 1 compares the typical compression isotherms of DPPC, DPPC:POPG (7:3), Survanta, Curosurf, Infasurf, BLES, and BNS. First, compression isotherms of all modified-natural surfactants and BNS feature a plateau region at π 40–50 mN/m. In contrast to these protein-containing surfactants, pure DPPC shows a well-characterized isotherm with a phase transition plateau at 3–5 mN/m [28,29], and DPPC:POPG shows no apparent plateau region. Due to the existence of the plateau, compression isotherms of modified-natural and natural surfactants can be separated into four regions, as indicated in Fig. 1. In the regions before and after reaching the plateau, surfactant films have a significantly lower film compressibility (i.e., less area reduction to increase π) than the plateau region. The fourth region refers to the film collapse plateau at which the surfactant films reach their maximum π. The molecular nature of these four regions is discussed below in combination with AFM observations. Second, the compression isotherms shift, after passing the plateau region, from right to left in the order of DPPC, DPPC:POPG, Survanta, Curosurf, Infasurf, BLES, and BNS. This order in general agrees with the rank of decreasing DPPC content in each preparation (see Table 1). Third, all surfactant films but Survanta collapse at π of ~72 mN/m, corresponding to near-zero surface tension at room temperature. Survanta, on the other hand, collapses at ~62 mN/m.

3.2. Comparison of film structures

Fig. 2 is a compilation of AFM images comparing micro- and nano-structures of different surfactant films obtained at increasing π. All surfactants, with the exception of DPPC, were studied at 20, 30, 40, 50, 60 mN/m, and the pressure at which the films collapse. In comparison, DPPC was studied at 2.8, 4.0, 10, 30, 60 and 72 mN/m. These characteristic pressures were selected to cover the complete

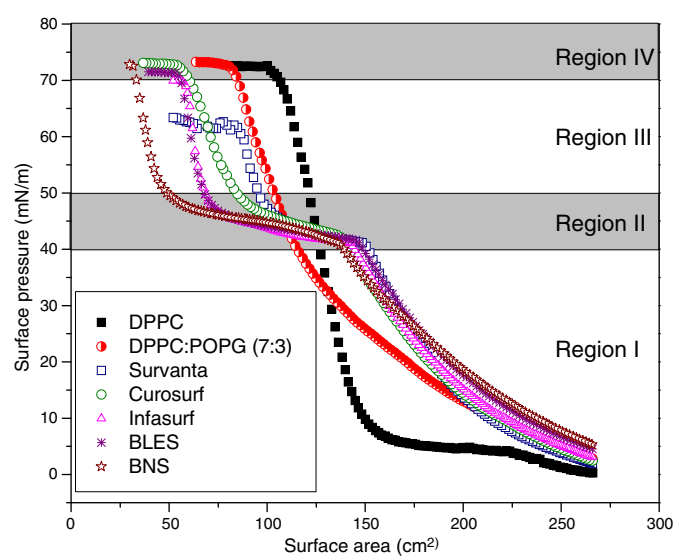

Fig. 1. Comparison of typical compression isotherms of various synthetic, modified-natural, and natural surfactant films at room temperature. The two protein-free synthetic systems are pure DPPC and DPPC:POPG (7:3). The four clinical modified-natural surfactants are Survanta, Curosurf, Infasurf, and BLES. The native natural surfactant for comparison is bovine natural surfactant (BNS). All pulmonary surfactants were spread as monolayers to an initial surface pressure (π) of 1–3 mN/m prior to compression. Surfactant films were compressed at an identical rate of 20 cm^2/min until film collapse. Four pressure-dependent regions are detected for the compression isotherms of protein-containing modified and natural surfactants. These are: Region I. Monolayer region at $\pi \leq 40$ mN/m; Region II. Monolayer-to-multilayer transition region at $40 < \pi < 50$ mN/m; Region III. Multilayer region at $\pi \geq 50$ mN/m; and Region IV. Collapse region at 72 mN/m for all films but Survanta, which collapses at 62 mN/m. The structural nature of these four regions is revealed in Fig. 2 by AFM.

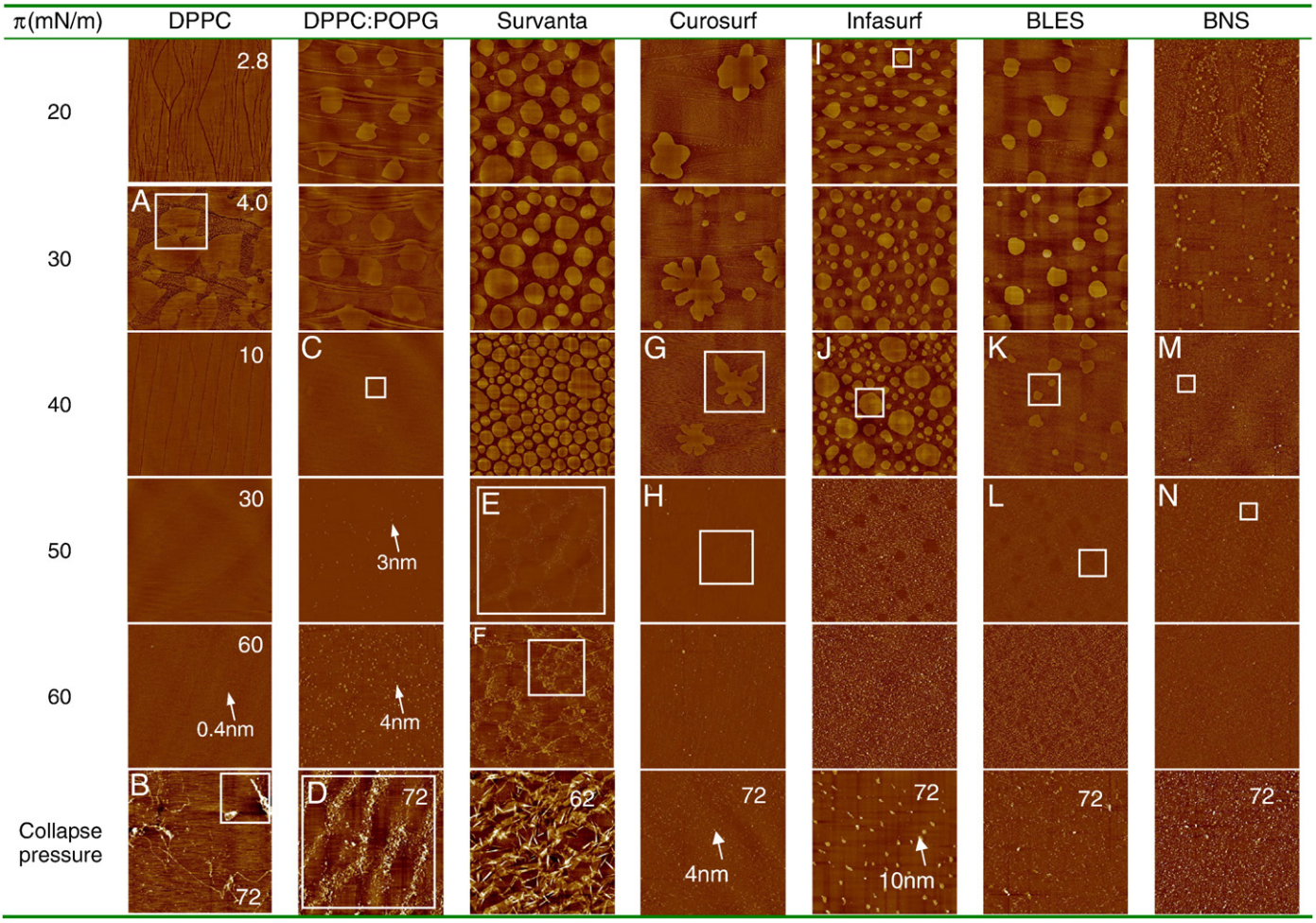

Fig. 2. Comparison of characteristic AFM topographic images of various synthetic, modified-natural, and natural surfactant films at increasing surface pressure (π). All surfactants but DPPC were studied at a series of π of 20, 30, 40, 50, 60 mN/m, and the π at which the film collapses, i.e., 72 mN/m for DPPC:POPG, Curosurf, Infasurf, BLES, and BNS, and 62 mN/m for Survanta. In comparison, DPPC was studied at π of 2.8, 4.0, 10, 30, 60 and 72 mN/m. These characteristic pressures were selected to cover the complete and detailed evolution of each surfactant film under compression, i.e., before, during and after the plateau region in the compression isotherm (Fig. 1). All AFM images were obtained with the same scan parameters, i.e., Setpoint = 1 V; PID Gains = 3/2/0; and Scan rate = 1 Hz. The AFM scan area was 50 × 50 μm for all images. For the purpose of comparison among different surfactants, the full *z*-range was set to be 5 nm for all images at $\pi \leq 40$ mN/m, and 20 nm for $\pi > 40$ mN/m (with the only exception being DPPC at 60 mN/m, the *z*-range was reduced to 5 nm to demonstrate topographic features). Relative height of critical structures is pointed by arrows. Critical lateral structures indicated by rectangular boxes are shown in high-resolution images in Fig. 3.

and detailed evolution of each surfactant film under compression. For the purpose of comparison, all AFM images were obtained with the same scan parameters, i.e., Setpoint = 1 V; PID Gains = 3/2/0; and Scan rate = 1 Hz. All images have the same scan area of 50 × 50 μm. The full *z*-range is 5 nm for all images at $\pi \leq 40$ mN/m (i.e., before reaching the plateau), and 20 nm for all images at $\pi > 40$ mN/m (i.e., after passing the plateau). The only exception is the DPPC image at 60 mN/m, which has a full *z*-range of 5 nm to demonstrate shallow features.

Fig. 3 shows selected height profiles, three-dimensional surface plots, and high-resolution AFM images, corresponding to regions indicated by boxes in Fig. 2. These images have different scan areas and *z*-ranges, adjusted for optimum presentation of detailed film structures.

3.2.1. DPPC

As shown in the first column of Fig. 2, pure DPPC remains a monolayer up to collapse at 72 mN/m. At a very low pressure of 2.8 mN/m, the DPPC monolayer is in a fluid-like liquid-expanded (LE) phase in which the phospholipid molecules have a low packing density and the fatty acid chains remain largely disordered and fluid [28,29]. At 4.0 mN/m, the DPPC monolayer shows well-defined chiral microdomains and small nanodomains [5,28–31]. The domain formation indicates coexistence of the LE phase with a more ordered and rigid tilted-condensed (TC) phase, which extends ~1 nm beyond the LE phase [5,21,32]. Note that when discussing phospholipid phase behavior we adopt the nomenclature proposed by Kaganer et al. [32], who suggest the use of TC phase to replace the commonly used liquid-condensed (LC) phase. The line tracing in Fig. 3A illustrates heights of microdomains and nanodomains, relative to the continuous LE phase. Both microdomains and nanodomains have the same height, indicating they are both in the TC phase [29–31]. The plateau shown in the DPPC isotherm at 3–5 mN/m therefore indicates a first-order phase transition [28,32]. After passing the phase transition plateau, the DPPC monolayer at 10 and 30 mN/m is primarily in a homogenous TC phase, thus with a very low film compressibility. When pressure is increased to 60 mN/m, a number of small "peaks" of only 0.4 nm high (indicated by the arrow) appear uniformly in the monolayer, indicating onset of monolayer destabilization under the extreme lateral compression. At 72 mN/m, the DPPC monolayer collapses completely, as indicated by the formation of a film collapse plateau in the isotherm and bilayer stacks (Fig. 3B) on top of the monolayer.

3.2.2. DPPC:POPG (7:3)

The second column of Fig. 2 shows the film structure of the protein-free binary model system DPPC:POPG (7:3). At 20 mN/m, the DPPC:POPG monolayer shows phospholipid phase separation. Lateral

chemical analysis in previous ToF-SIMS experiments proved that the TC domains consist of DPPC and the surrounding LE phase contains less ordered POPG [33–35]. In addition to the circular domains, there are stripes with the same height as the TC domains and organized in the direction perpendicular to the dipping direction. Similar phenomenon is also found for Curosurf. It appears that these stripes are not due to an AFM tip artifact as they remain unchanged as varying scan direction, rate, and force, or using different scan modes. These might be due to an artifact of LB transfer in which substrate-mediated condensation occurs during or after the transfer [36]. However, the reason why this artifact

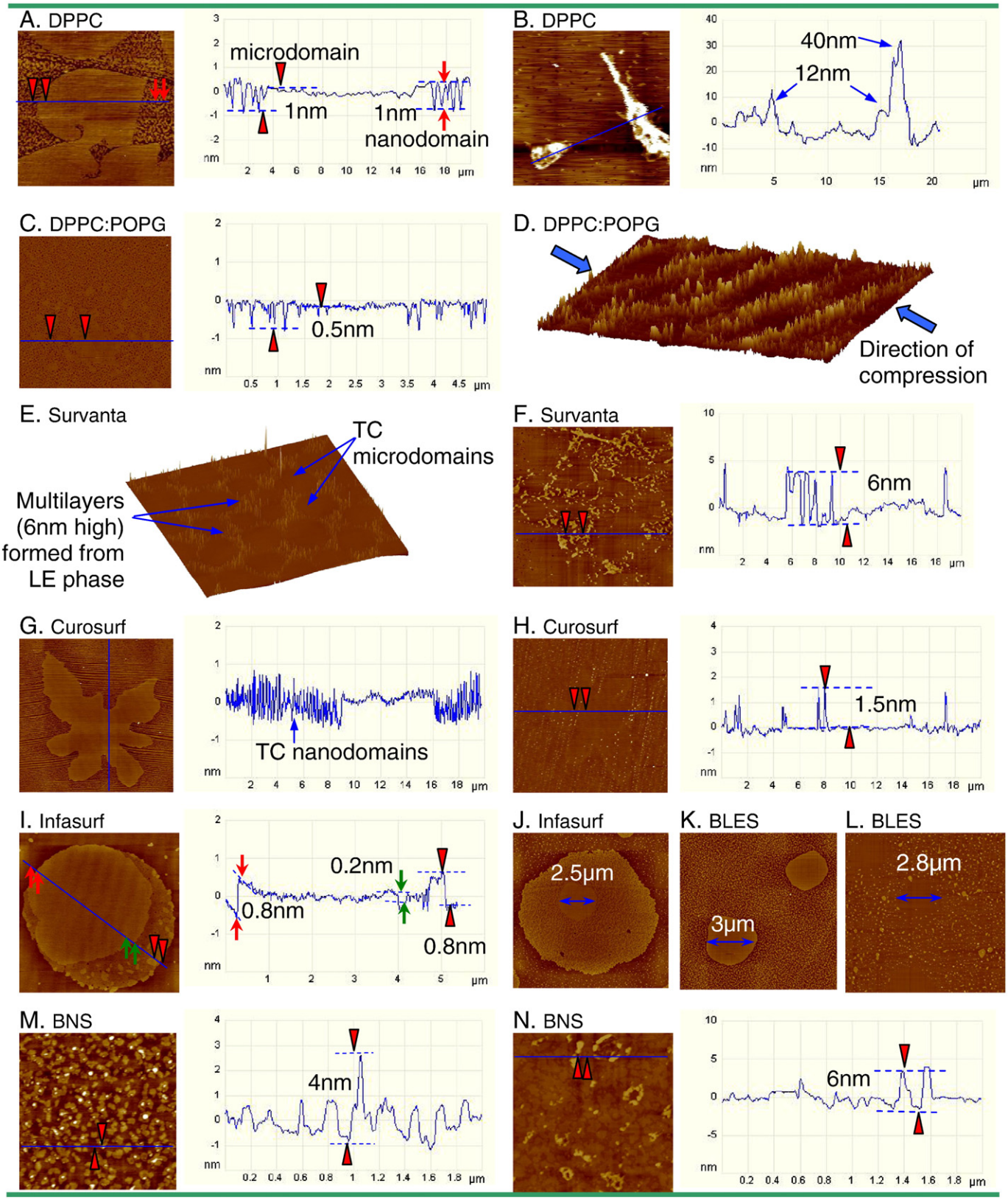

seems to be less detectable for the other surfactant preparations is unknown.

With pressure increase to 30 mN/m, the TC domains grow in size. At 40 mN/m, the TC domains become less detectable in the topographic image. A closer look at the film (Fig. 3C) confirms that the TC domains are packed together to form a somewhat continuous phase with "holes" of ~0.5 nm in depth, likely due to the trapped LE phase. It appears that further increasing pressure to 50 mN/m induces formation of isolated bilayer structures (~3 nm in height, as pointed by the arrow) attached to the interfacial monolayer, due to localized film collapse. The multilayer structures grow in the lateral dimension but not significantly in height (~4 nm as pointed) with further increasing pressure to 60 mN/m. The film eventually collapses at 72 mN/m, where patterns of film folding are clearly observed along the direction of film compression (Fig. 3D).

3.2.3. Survanta

Survanta is prepared from minced bovine lung tissue, extracted with chloroform-methanol, and further purified by precipitation with ethyl acetate. These purification procedures result in a loss of cholesterol and a reduction in SP-B [15,17]. Due to its relatively poor capacity in reducing surface tension, Survanta is further supplemented with synthetic DPPC, palmitic acid and tripalmitin. As shown in the third column of Fig. 2, Survanta monolayers at 20 mN/m present a clear TC-LE phase separation, indicated by formation of round-shaped TC domains mainly in the micrometer size. The area coverage of the TC phase increases continuously with increasing pressure up to 40 mN/m (Fig. 4). At 50 mN/m, i.e., immediately past the plateau in the compression isotherm, the original monolayer is transformed into multilayers. A surface plot at 50 mN/m (Fig. 3E) demonstrates that a matrix of multilayers (about two bilayers high relative to the surface monolayer) is formed surrounding the TC domains in the interfacial monolayer. Similar structure of Survanta has been reported by another group [37]. This film structure strongly implies that the multilayers must be initiated from the LE phase in the original surfactant monolayers. As π is increased to 60 mN/m, the multilayers mainly grow in the lateral dimension but not in the altitudinal direction (Fig. 3F); while the TC domains in the interfacial monolayer are further packed. At 62 mN/m, the Survanta film permanently collapses and forms localized folding structures in arbitrary orientations, which differs from the whole-film, orientational folding of DPPC:POPG film at its collapse pressure.

3.2.4. Curosurf

Curosurf is prepared from minced porcine lung tissue. It is depleted of cholesterol by undergoing gel-chromatography to remove all neutral lipids during manufacture [4]. As shown in the fourth column of Fig. 2, the Curosurf monolayer at 20 mN/m exhibits significantly fewer, but larger, noncircular domains, compared to Survanta, presumably indicating a higher film viscosity [38,39]. With increasing π, the domain shape becomes more ramified. Nanodomains with the same height of microdomains tend to line up horizontally to form stripes (Fig. 3G). As pressure is increased to 50 mN/m, the Curosurf film displays moderate

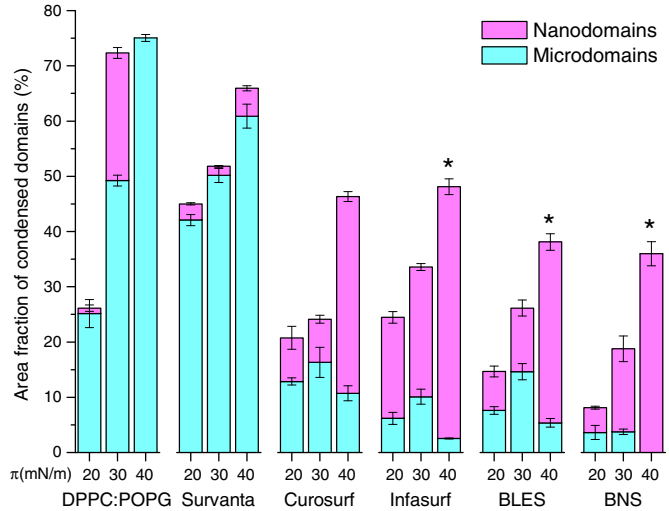

Fig. 4. Quantification results of monolayer coverage of tilted-condensed (TC) domains upon film compression. Monolayers of DPPC:POPG (7:3), Survanta, Curosurf, Infasurf, BLES, and BNS were quantified at surface pressures (π) of 20, 30, and 40 mN/m. At each pressure, area fractions of microdomains, nanodomains, and total TC domains (sum of micro- and nano-domains) were quantified with image analysis. $^{*}P<0.05$ for differences between area fractions of microdomains at 30 and 40 mN/m, for Infasurf, BLES, and BNS.

(only ~1.5 nm high) buckling along the direction of lateral compression (Fig. 3H). At 60 mN/m and even 72 mN/m where the film ultimately collapses, the multilayer structures only grow slightly to ~4 nm high, indicating very limited film collapse and high film stability.

3.2.5. Infasurf

Infasurf is prepared from lung lavage of newborn calves by centrifugation and organic solvent extraction, and it contains all of the hydrophobic components of natural surfactant. Compared to Survanta and Curosurf, Infasurf has a high cholesterol content (Table 1). It is well known that cholesterol has a profound influence on the phase behavior of phospholipid monolayers and membranes [5,40–43]. Depending on its ratio to phospholipids in monolayers, cholesterol can selectively partition into TC phase phospholipid domains and induce a new liquid-ordered (LO) phase, whose degree of lipid chain order is intermediate between the LE and TC phases [5,40–43]. As shown in the fifth column of Fig. 2, all three phases (i.e., LE, LO, and TC) are detected in the Infasurf monolayer. As a consequence of partitioning into the TC domains, the high cholesterol content in Infasurf results in a unique domain-in-domain (TC-in-LO) structure. In Fig. 3I, scanning from left to right, one observes the background LE phase, a microscale TC domain 0.8 nm higher than the LE phase, a LO phase 0.2 nm lower than the TC phase, and nanoscale TC domains 0.8 nm higher than the surrounding LE phase. These height variations are in good agreement with the relative chain order of these three phases.

Fig. 3. High-resolution AFM images, as indicated by rectangular boxes in Fig. 2, demonstrating detailed structural features of surfactant films. A. DPPC monolayer at 4.0 mN/m. The height profile shows the surface topography along the line tracing indicated in the AFM image. It shows that the tilted-condensed (TC) phase consists of both leaf-like microdomains and worm-like nanodomains, both ~1 nm higher than the surrounding liquid-expended (LE) phase. B. Collapsed DPPC monolayer at 72 mN/m, showing the formation of bilayer stacks ejected from the interfacial monolayer at the collapse pressure. C. Monolayer of DPPC:POPG (7:3) at 40 mN/m, showing that the condensed domains merge into a continuous phase with "holes" of LE phase ~0.5 nm lower. D. Surface plot (three-dimensional topographic image) of DPPC:POPG film at the collapse pressure (i.e., 72 mN/m), showing film folding along the direction of lateral compression. E. Surface plot of Survanta film at 50 mN/m. It shows that the TC microdomains are traced out by higher multilayers that originate from the surrounding LE phase. F. Survanta film at 60 mN/m, illustrating an increasing multilayer density in the lateral dimension while the height of multilayers does not increase significantly, compared to 50 mN/m. G. Curosurf monolayer at 40 mN/m shows a single microdomain with lines of nanodomains, as indicated by the intensive fluctuations in the height profile. H. Curosurf film at 50 mN/m, showing a single TC microdomain with moderate film buckling, indicated by vertical lines of collapse sites of only ~1.5 nm high. I. Infasurf monolayer at 20 mN/m shows the cholesterol-mediated liquid-ordered (LO) phase and a unique TC-in-LO structure as a consequence of cholesterol partitioning into the TC phospholipid phase. The lipid chain order of the LO phase is intermediate between the TC and LE phases, as indicated by height differences detected by AFM (i.e., TC>LO>LE in height). J. Infasurf monolayer at 40 mN/m, demonstrating a single TC-in-LO domain with an increasing number of nanodomains and evident shrink of the TC core (2.5 μm vs. 5 μm at 30 mN/m). K. BLES monolayer at 40 mN/m, showing clearly a decrease of microdomains in size and increase of nanodomains in number. L. BLES film at 50 mN/m, showing TC microdomains traced out by multilayers formed from the surrounding LE phase. M. BNS monolayer at 40 mN/m, showing the detailed morphology of nanodomains and some high spots, likely SP-A aggregates squeezed out of the monolayer at this pressure. N. BNS film at 50 mN/m, showing detailed multilayer structure.

Upon increasing pressure, the TC microdomains (i.e., the higher core of the TC-in-LO phase) first increase in size as pressure increases from 20 to 30 mN/m, and then decrease in size as pressure increases from 30 to 40 mN/m. Fig. 3J is a high resolution image that demonstrates evident shrinkage of the TC microdomains at 40 mN/m. With further increasing pressure to 50 mN/m, the Infasurf monolayer is transformed into multilayers (~6 nm higher than the surface monolayer). Similar to Survanta, the multilayers clearly encompass the TC microdomains in the interfacial monolayer, which indicates that the multilayers stem from the LE (and possibly also the LO) phase in the original monolayer. Upon increasing pressure to 60 mN/m, the multilayers are closely packed in the lateral dimension but do not significantly increase in height. At 72 mN/m, a few isolated protrusions of ~10 nm high appear. Since AFM measures relative height, these protrusions are 10 nm higher than the tightly packed multilayers in the background. This collapse mechanism is quite different from the folding mechanism of the model system, Survanta and Curosurf.

3.2.6. BLES

BLES is prepared from adult cows being slaughtered for food with a foaming procedure, followed by organic solvent extraction [22]. BLES is similar to Infasurf in phospholipid and protein profiles (Table 1). However, BLES has a reduced cholesterol content as it undergoes an acetone extraction. Under the current manufacturing process, the final cholesterol content in BLES is 2–3% [44], i.e., one-third to one-half of that in bovine natural surfactant. As shown in the sixth column of Fig. 2, BLES films generally consist of LE and TC phases, due to the reduced cholesterol content (note that few domain-in-domain structures appear only at 20 mN/m). Similar to Infasurf, the TC microdomains in BLES first increase from pressures of 20 to 30 mN/m, and then decrease from 30 to 40 mN/m. Associated with the decrease of microdomains is a significant increase in the number of nanodomains (Fig. 3K). This pressure-dependent domain conversion is in good agreement with our previous study of BLES [21]. It is also clear that the multilayers at 50 mN/m originate from the LE phase and encompass the TC microdomains (Fig. 3L). Topographical analysis shows that the multilayered protrusions consist of stacked bilayers of 5–6 nm high. The formation of multilayers at 50 mN/m is also consistent with previous AFM studies using BLES and model surfactants [21,41,45–52]. Nevertheless, the multilayered protrusions detected in the present study seem to be smaller than those found previously with BLES [21,46,51,52]. This might be due to batch-to-batch variations of animal-derived preparations. With further increasing pressure, the multilayers pack tightly and finally collapse at 72 mN/m as individual protrusions (~12 nm), similar to the collapse mechanism of Infasurf.

3.2.7. Bovine natural surfactant

The last column of Fig. 2 shows the structure of bovine natural surfactant (BNS), which contains the full spectrum of surfactant phospholipids, 5–8% cholesterol, and both hydrophobic (SP-B/C) and hydrophilic (SP-A) proteins (Table 1). Different from both model system and modified-natural surfactants used in clinical practice, the domain size in BNS is primarily in the nanometer range. Especially at 40 mN/m, only nanodomains appear at the monolayer. Some high spots, measured to be ~4 nm in height, appear at 40 mN/m (Fig. 3M). These high spots are likely to be SP-A aggregates squeezed out of the monolayer at this pressure [21]. All these observations are in good agreement with our previous work of recombinant BLES with 5% SP-A [21]. Multilayer structures of ~6 nm in height appear at 50 mN/m (Fig. 3N) and are packed closely at 60 mN/m. At 72 mN/m, BNS shows significantly higher collapse protrusions (~32 nm) compared to Infasurf and BLES.

3.3. Quantitative analysis of condensed domains

Fig. 4 shows quantification results for the condensed phospholipid domains (i.e., the TC phase) in micrometer-size (microdomains) and nanometer-size (nanodomains) for all surfactant monolayers, excluding DPPC. The quantification is limited to monolayers, i.e., at $\pi \leq 40$ mN/m. At higher pressures, the formation of multilayers prevents accurate quantification of domain areas, especially nanodomains, at the interfacial monolayer.

As shown in Fig. 4, the total area fraction of condensed domains (combined microdomains and nanodomains) increases for all surfactant preparations with increasing pressure from 20 to 40 mN/m. The total area fraction of condensed domains at 40 mN/m is approximately equal to the fraction of disaturated phospholipids (mainly DPPC) in each surfactant preparation (Table 1). In contrast to the monotonic increase of total condensed domains, the pressure-dependence of microdomains and nanodomains varies between different surfactant preparations. For DPPC:POPG and Survanta, the microdomains are predominant, especially at 40 mN/m, i.e., the onset of monolayer-to-multilayer transition. In contrast, in the monolayers of Curosurf, Infasurf, BLES, and BNS, nanodomains represent the major fraction of condensed phase at 40 mN/m. Importantly, there is a significant decrease ($P<0.05$) of area fraction of microdomains and increase of nanodomains upon pressure increase from 30 to 40 mN/m, in Infasurf, BLES and BNS, i.e., the three surfactant preparations that contain cholesterol.

4. Discussion

Langmuir monolayers self-assembled at the air–water interface are an established *in vitro* model of studying biophysical properties of pulmonary surfactant [5,19,41,53–55]. Film imaging with AFM obtains direct topographical features of these surfactant films. Interpretation of the film topography in terms of lateral structure and molecular organization is based on well-established experimental evidence obtained from molecular characterization techniques, such as fluorescence microscopy and ToF-SIMS [5,18–21,33–35].

It is found that although all clinical surfactants exhibit similar film compressibility, they show very different lateral structure and molecular organization (Figs. 2 and 3). These differences are largely due to the different biochemical compositions of animal-derived preparations, which are consequences of varied animal sources (bovine vs. porcine) and production procedures (bronchopulmonary lavage vs. lung mincing) [4]. As shown in Table 1, clinical surfactant preparations differ in phospholipids, cholesterol, individual surfactant proteins (SP-B and SP-C), and additives (such as free fatty acids). Here, we limit our discussion on only two surfactant components, DPPC and cholesterol. However, it should be noted that the exclusion of surfactant proteins from the discussion is not to deemphasize their effects. It is well known that SP-B and SP-C play a crucial role in monolayer-to-multilayer transition upon film compression, adsorption and readsorption/respreading of surfactant film upon film expansion [5,41,49,56–58]. Recent mechanistic studies have shown that although at a small content (<2 wt.%), these two hydrophobic proteins may function collaboratively or independently and most likely in synergy with cholesterol in optimizing the biophysical properties of pulmonary surfactant [59–61].

According to their compression isotherms, we have identified four π-dependent regions for all protein-containing modified and natural surfactants. As noted in Fig. 1, these four regions, based on film structures revealed by AFM, are referred to as I, monolayer region; II, monolayer-to-multilayer transition region; III, multilayer region; and IV, collapse region.

4.1. Region I. Phospholipid phase separation in surfactant monolayers

At π lower than ~40 mN/m, modified and natural surfactants are in monolayers. Surfactant monolayers in this region are conceivably of no significant physiological relevance as surface tension in the lungs during normal tidal breathing most likely varies from near-zero to not

much higher than 30 mN/m, corresponding to a π range of ~40–70 mN/m [62]. However, surfactant monolayer in this region may be germane to certain abnormal and disease conditions marked with elevated alveolar surface tension due to surfactant deficiency and/or dysfunction [63].

First, we found that at the onset of monolayer-to-multilayer transition (i.e., 40 mN/m), the total area fractions of condensed domains for all surfactant preparations are approximately equal to the molecular fraction of disaturated phospholipids (mainly DPPC) in each individual surfactant. This observation suggests that 1) there is no alteration of chemical composition of monolayers within Region I, and 2) regardless of their specific contents, DPPC molecules in all surfactant preparations are fully packed into a rigid and ordered TC phase up to 40 mN/m.

Second, we found that cholesterol plays an important role in regulating the phospholipid phase behavior in surfactant monolayers. With 5–8% in weight or 10–16% in mole, cholesterol induces a new phase in Infasurf monolayers, indicated by the appearance of a unique domain-in-domain structure. A similar structure has been reported in BLES supplemented with extra cholesterol [64] and in rat surfactant that contains ~8 wt.% cholesterol [44]. Our topographic analysis indicates this domain-in-domain structure to be a TC-in-LO phase. This composition–structure interpretation is also supported by previous evidence of this structure disappearing after cholesterol extraction and reappearing with cholesterol supplementation [44,64]. The concept of cholesterol-mediated LO phase in surfactant monolayers is extended from the study of cholesterol-containing bilayers [5,41]. Ipsen et al. proposed that cholesterol intercalates in lipid bilayers to regulate lipid chain order [65]. Consequently, the fluidity and other biophysical properties of the resultant liquid-ordered (L_o) phase in bilayers are intermediate between the liquid-disordered (L_d) phase (i.e., the bilayer counterpart of the LE phase) and the solid-ordered (S_o) phase (i.e., the bilayer counterpart of the TC phase) [42,43,65]. It should also be noted that the cholesterol concentration in Infasurf falls into the range of S_o–L_o phase coexistence at sub-melting temperature, as indicated by the generic binary phase diagram [42,43,65]. Therefore, the formation of LO phase in Infasurf monolayers is not completely unexpected.

In addition, we demonstrated dissolution of TC microdomains at 40 mN/m in all cholesterol-containing surfactants (Infasurf, BLES, BNS) but not in cholesterol-free surfactants (DPPC:POPG, Survanta, and Curosurf). This phenomenon was previously referred to as phase remixing, a process attributed to cholesterol [66]. Our recent study with BLES suggested that the dissolution of TC microdomains was at the expense of increasing nanodomains [21], which is also confirmed in this study with Infasurf and BNS. Interestingly, high-resolution AFM reveals that phase remixing may be regulated by the cholesterol-mediated LO phase in the monolayer, which facilitates dissolution of TC microdomains into nanodomains upon increasing π (Figs. 3I vs. 3J), presumably by reducing line tension at the domain boundaries [21,66]. The dissociation of TC microdomains into nanodomains significantly enhances the uniformity of phase coexistence at the interfacial monolayer, thus promoting the subsequent squeeze-out of fluid phospholipids into multilayered protrusions upon further compression in Region II.

4.2. Region II. Monolayer-to-multilayer transition at the equilibrium spreading pressure

At π between ~40 and ~50 mN/m, modified and natural surfactants are in a transition state from a monolayer to a multilayer. Surface pressure in this range, or ~45 mN/m representatively, is the equilibrium spreading pressure (π_e) of fluid phospholipids, at which fully-hydrated phospholipid vesicles reach equilibrium with the phospholipid monolayer at the air–water interface [5]. The π_e is also the maximum π that can be reached by fully-hydrated phospholipid vesicles during adsorption or spreading. Further increasing π, if possible, can be only achieved by lateral film compression. Molecular structure in this region could represent the surfactant film formed by *de novo* adsorption of endogenous surfactant, or by spreading of exogenous clinical surfactants.

Our study provides direct experimental evidence of film refining due to selective squeeze-out of the fluid components at this pressure range. First, we have shown that compression isotherms of different modified and natural surfactants in this region shift to the left in the order of decreasing DPPC content. As a result, a longer plateau or more area reduction is required to refine a monolayer containing a higher amount of non-DPPC components. Second, AFM reveals a squeeze-out process in monolayers of Survanta, Infasurf and BLES. It is shown that multilayers at 50 mN/m originate from the LE phase and encompass the TC microdomains in the interfacial monolayer. These AFM observations are supported by recent chemical characterization of BLES using ToF-SIMS, which revealed that the lower domains consist of disaturated phospholipids (mainly DPPC) and the surrounding higher phase is enriched in unsaturated phospholipids [19]. Selective squeeze-out of fluid components (those with lower π_e) from multicomponent phospholipid monolayers is a well studied physicochemical phenomenon [67]. The squeeze-out process in monolayers of protein-containing surfactants was found to be reversible [5,67]. In this way, the squeezed out multilayers form a surface-associated surfactant reservoir for effective film replenishment during expansion.

Curosurf has the highest amount of phospholipids and lowest amount of neutral lipids in all clinical surfactant preparations. Different from the others, monolayers of Curosurf in this pressure range display only moderate film buckling along the direction of lateral compression. This may be related to the nonuniform phase coexistence at its interfacial monolayer. With a significantly large domain size and lack of cholesterol-mediated microdomain-to-nanodomain conversation, monolayers of Curosurf intrinsically lack nucleation sites for the reversible collapse, usually occurring at the domain boundaries [67,68].

4.3. Region III. Metastable monolayer with attached multilayers

At π above π_e but before reaching the ultimate film collapse, surfactant films are in a metastable state with an interfacial monolayer attached with squeezed out multilayers. This region covers a π range from ~50 to 72 mN/m, most likely representing the physiologically relevant π range. It should be noted that although surfactant films in this region are in a multilayer structure, surface activity must still be controlled by the interfacial monolayer. The fact that all natural surfactant films show very low compressibility similar to that of DPPC monolayers in this region indicates the interfacial monolayers must be enriched with DPPC in the TC phase. Importantly, with increasing π to 60 mN/m, we found that multilayer structures increase density in the lateral dimension but do not significantly grow in height. This observation indicates that the film refining process (i.e., selective squeeze-out) is largely completed during the plateau region. With further compression, the interfacial monolayer already enriched in DPPC (as well as the attached multilayers) is further packed to decrease surface tension to near-zero. How pulmonary surfactant films reach low surface tension has remained an open question [5,54,55]. Our present data provide direct experimental evidence in support of a detailed biophysical mechanism of combined phospholipid phase separation and multilayer formation due to squeeze-out of fluid phospholipid components.

4.4. Region IV. Collapse mechanisms of surfactant films

Collapse pressure (π_c) is the maximum π that can be reached and sustained by a phospholipid film under lateral compression. At π_c, surfactant films irreversibly collapse by excluding phospholipid vesicles of the *same* composition as the interfacial monolayers. This process is

essentially different from the *selective* and reversible squeeze-out of fluid components from the interfacial monolayer at π_e. In mammal lungs, ultimate film collapse at π_c, if any, may only be limited and transient at end-expiration as this process is not energetically favorable. We found that all surfactant films but Survanta collapse at π ~72 mN/m, corresponding to a near-zero surface tension. The early collapse of Survanta films has been well-documented [15–17]. Compared to other clinical preparations, Survanta lacks SP-B (Table 1). However, monolayers of synthetic model surfactant (DPPC:POPG) without surfactant proteins collapse at 72 mN/m. Hence, the early collapse of Survanta films might be due to the supplemented palmitic acid components because monolayers of palmitic acid collapse on a pure water subphase at only ~50 mN/m [69].

We found that cholesterol also plays a role in regulating the collapse mechanism of surfactant films. Surfactant films without cholesterol (DPPC:POPG, Survanta, and Curosurf) appear to collapse with a folding mechanism, like an elastic sheet. In contrast, surfactant films with cholesterol (Infasurf, BLES, and BNS) appear to collapse with a protrusion mechanism, in which multilayered protrusions are uniformly nucleated throughout the entire film. The cholesterol-regulated film collapse mechanism may be best explained by fusion pore formation [19] and/or variations in film fluidity [70], as also suggested by molecular dynamics simulations [71,72].

4.5. Clinical implications

Deficiency and/or dysfunction of pulmonary surfactant are involved in many airway, parenchymal, and interstitial lung diseases [63]. In addition to its success in treating RDS, surfactant therapy in recent years has been applied to a variety of neonatal, pediatric, and adult respiratory conditions [2,3,73], such as the chronic lung disease (also known as bronchopulmonary dysplasia) [74], asthma [75,76], meconium aspiration syndrome [77], neonatal pulmonary hypertension, congenital pneumonia, congenital diaphragmatic hernia, pulmonary hemorrhage [2,3,73], acute lung injury and acute respiratory distress syndrome [78]. Although more studies are needed to establish the efficacy of surfactant therapy for many of these conditions, clinical surfactants appear to be a promising and versatile therapeutic intervention [2,3,73,74]. It should be noted that new applications for clinical surfactants are still emerging [79,80], including their use as a carrier to deliver corticosteroids directly to the lungs of premature newborns with or at high risk for chronic lung disease [81]. Therefore, it is of vital importance to characterize and compare exogenous surfactant preparations currently available for clinical practice, both biochemically and biophysically. *In vitro* characterization of composition–structure correlation of surfactant films can also provide implications for the development of new generation synthetic designer surfactants.

To date, no synthetic surfactant available can confer a comparable biophysical and clinical performance as the animal-derived preparations [3–5]. Two new generation synthetic surfactants that contain a simple peptide or protein analogs, Surfaxin and Venticute, both rely on DPPC:POPG (~7:3) as the lipid skeleton [3–5]. DPPC is the only major phospholipid component in pulmonary surfactant with a bilayer transition temperature above the core body temperature [5]. Therefore, it has long been considered to be the main surface active component in pulmonary surfactant. However, recent comparative biology studies suggested that the DPPC content is highly variable among mammals and it is even not the major phospholipid in some species [24,82]. The DPPC content also varies significantly in different animal-derived clinical surfactants, from ~40% in BLES to ~50% in Survanta (Table 1). In spite of this variation in DPPC content, clinical superiority in terms of statistical differences in mortality or days in neonatal intensive care units related to difference surfactant preparations has not been established [3–5].

Our AFM observations found that regardless of the DPPC content of a particular surfactant preparation, all clinical surfactant films assume a similar molecular organization at the physiologically relevant surface tension range, i.e., multilayers of fluid phospholipids closely attached to an interfacial monolayer enriched in DPPC. This film structure results from a refining process around π_e, at which surfactant films are formed *in vivo* either by adsorption of the endogenous surfactant or by spreading of the exogenous surfactant.

Our data therefore suggest that a high content of DPPC may not necessarily be crucial for designing a synthetic surfactant. Actually, a high DPPC content may compromise the biophysical properties, especially adsorption, of a surfactant substitution. This view is in line with that of Holm et al. who showed that increasing DPPC content to 60% or 80% in a model system did not increase dynamic surface activity but compromised adsorption [83]. This may also explain the limited success of synthetic surfactants enriched with DPPC, such as Exosurf and ALEC. In view of balancing surface tension lowering ability and rapid adsorption, it might be desirable to design a functional synthetic surfactant with the lowest possible DPPC content. The threshold DPPC content is still to be determined, but it appears that 40% DPPC as in bovine natural surfactant is sufficient to maintain adequate biophysical properties with the aid of hydrophobic surfactant proteins.

Being a minor lipid component with limited analysis in the past, the role of cholesterol in pulmonary surfactant has attracted significant attention in recent years [40,44,46,64,84]. Our data suggest that a cholesterol content as low as 2–3% (as in BLES) can induce significant variation in surfactant films, including formation of cholesterol-mediated phospholipid phases, variation of film fluidity and collapse mechanism. Although cholesterol at a supraphysiological level exhibits significant inhibition on surfactant function, cholesterol at the physiological level or lower appears not to affect the surface tension lowering ability [46,50,64,84,85]. Therefore, cholesterol-free surfactant preparations might be more efficacious for treating certain conditions such as ARDS, in which an elevated level of cholesterol is found in the bronchoalveolar lavage fluid of these patients [86,87].

5. Conclusions

We report the first comprehensive characterization and comparison of micro- and nano-structures of all major animal-derived clinical surfactant preparations using AFM. This comparative study reveals the composition–structure correlation of clinical surfactants as well as the biophysical mechanisms of pulmonary surfactant films in response to lateral compression. This study may have implications for clinical applications of surfactant preparations and translational value for the development of new generation synthetic designer surfactants.

Acknowledgments

The authors thank Zdenka Policova at the University of Toronto for conducting the phosphorus assay of bovine natural surfactant. The authors are grateful to Profs. Fred Possmayer and Ruud Veldhuizen at the University of Western Ontario and Prof. David Easa at the University of Hawaii for critical review of the manuscript. Samples of BLES, Infasurf, and Curosurf were gifts from Dr. Harold Dick at BLES Biochemicals Inc., Dr. Walter Klein at ONY Inc., and Dr. Alan Roberts at Cornerstone Therapeutics Inc., respectively. This work was supported by startup grants from the University of Hawaii at Manoa (Y.Y.Z) and the Leahi Fund to Treat & Prevent Pulmonary Disease (44936) from the Hawaii Community Foundation (Y.Y.Z). H.Z. was supported by a faculty exchange program between Peking University and the University of Hawaii at Manoa, operated by the Center for Chinese Studies.

References

[1] T. Fujiwara, H. Maeta, S. Chida, T. Morita, Y. Watabe, T. Abe, Artificial surfactant therapy in hyaline-membrane disease, Lancet 1 (1980) 55–59.
[2] W.A. Engle, the Committee on Fetus and Newborn, Surfactant-replacement therapy for respiratory distress in the preterm and term neonate, Pediatrics 121 (2008) 419–432.
[3] H.L. Halliday, Surfactants: past, present and future, J. Perinatol. 28 (Suppl 1) (2008) S47–S56.
[4] O. Blanco, J. Perez-Gil, Biochemical and pharmacological differences between preparations of exogenous natural surfactant used to treat respiratory distress syndrome: role of the different components in an efficient pulmonary surfactant, Eur. J. Pharmacol. 568 (2007) 1–15.
[5] Y.Y. Zuo, R.A. Veldhuizen, A.W. Neumann, N.O. Petersen, F. Possmayer, Current perspectives in pulmonary surfactant-inhibition, enhancement and evaluation, Biochim. Biophys. Acta 1778 (2008) 1947–1977.
[6] H.L. Halliday, Overview of clinical trials comparing natural and synthetic surfactants, Biol. Neonate 67 (Suppl 1) (1995) 32–47.
[7] R.H. Pfister, R.F. Soll, T. Wiswell, Protein containing synthetic surfactant versus animal derived surfactant extract for the prevention and treatment of respiratory distress syndrome, Cochrane Database Syst. Rev. (2007) CD006069.
[8] F. Moya, A. Maturana, Animal-derived surfactants versus past and current synthetic surfactants: current status, Clin. Perinatol. 34 (2007) 145–177.
[9] S. Sinha, F. Moya, S.M. Donn, Surfactant for respiratory distress syndrome: are there important clinical differences among preparations? Curr. Opin. Pediatr. 19 (2007) 150–154.
[10] H.L. Halliday, Recent clinical trials of surfactant treatment for neonates, Biol. Neonate 89 (2006) 323–329.
[11] N. Seger, R. Soll, Animal derived surfactant extract for treatment of respiratory distress syndrome, Cochrane Database Syst. Rev. (2009) CD007836.
[12] R. Ramanathan, Animal-derived surfactants: where are we? The evidence from randomized, controlled clinical trials, J. Perinatol. 29 (Suppl 2) (2009) S38–S43.
[13] R. Soll, E. Ozek, Multiple versus single doses of exogenous surfactant for the prevention or treatment of neonatal respiratory distress syndrome, Cochrane Database Syst. Rev. (2009) CD000141.
[14] T.P. Stevens, E.W. Harrington, M. Blennow, R.F. Soll, Early surfactant administration with brief ventilation vs. selective surfactant and continued mechanical ventilation for preterm infants with or at risk for respiratory distress syndrome, Cochrane Database Syst. Rev. (2007) CD003063.
[15] W. Bernhard, J. Mottaghian, A. Gebert, G.A. Rau, H.H. von Der, C.F. Poets, Commercial versus native surfactants. Surface activity, molecular components, and the effect of calcium, Am. .J Respir. Crit. Care Med. 162 (2000) 1524–1533.
[16] M. Rudiger, A. Tolle, W. Meier, B. Rustow, Naturally derived commercial surfactants differ in composition of surfactant lipids and in surface viscosity, Am. J. Physiol. 288 (2005) L379–L383.
[17] R.H. Notter, Z. Wang, E.A. Egan, B.A. Holm, Component-specific surface and physiological activity in bovine-derived lung surfactants, Chem. Phys. Lipids 114 (2002) 21–34.
[18] A.G. Serrano, J. Perez-Gil, Protein–lipid interactions and surface activity in the pulmonary surfactant system, Chem. Phys. Lipids 141 (2006) 105–118.
[19] F. Possmayer, S.B. Hall, T. Haller, N.O. Petersen, Y.Y. Zuo, J. Bernardino de la Serna, A.D. Postle, R.A.W. Veldhuizen, S. Orgeig, Recent advances in alveolar biology: some new looks at the alveolar interface, Respir. Physiol. Neurobiol. 173 (2010) S55–S64.
[20] Y.Y. Zuo, S.M. Tadayyon, E. Keating, L. Zhao, R.A. Veldhuizen, N.O. Petersen, M.W. Amrein, F. Possmayer, Atomic force microscopy studies of functional and dysfunctional pulmonary surfactant films, II: albumin-inhibited pulmonary surfactant films and the effect of SP-A, Biophys. J. 95 (2008) 2779–2791.
[21] Y.Y. Zuo, E. Keating, L. Zhao, S.M. Tadayyon, R.A. Veldhuizen, N.O. Petersen, F. Possmayer, Atomic force microscopy studies of functional and dysfunctional pulmonary surfactant films. I. Micro- and nanostructures of functional pulmonary surfactant films and the effect of SP-A, Biophys. J. 94 (2008) 3549–3564.
[22] S. Yu, P.G. Harding, N. Smith, F. Possmayer, Bovine pulmonary surfactant: chemical composition and physical properties, Lipids 18 (1983) 522–529.
[23] K. Rodriguez-Capote, F.X. McCormack, F. Possmayer, Pulmonary surfactant protein-A (SP-A) restores the surface properties of surfactant after oxidation by a mechanism that requires the Cys6 interchain disulfide bond and the phospholipid binding domain, J. Biol. Chem. 278 (2003) 20461–20474.
[24] R. Veldhuizen, K. Nag, S. Orgeig, F. Possmayer, The role of lipids in pulmonary surfactant, Biochim. Biophys. Acta 1408 (1998) 90–108.
[25] E.G. Bligh, W.J. Dyer, A rapid method of total lipid extraction and purification, Can. J. Biochem. Physiol. 37 (1959) 911–917.
[26] N.J. Hardy, T.H. Richardson, F. Grunfeld, Minimising monolayer collapse on Langmuir troughs, Colloids Surf. A Physicochem. Eng. Aspects 284–285 (2006) 202–206.
[27] P. Eaton, P. West, Atomic Force Microscopy, Oxford University Press, New York, 2010.
[28] C.W. McConlogue, T.K. Vanderlick, A close look at domain formation in DPPC monolayers, Langmuir 13 (1997) 7158–7164.
[29] C.W. Hollars, R.C. Dunn, Submicron structures in I-alpha dipalmitoylphosphatidylcholine monolayers and bilayers probed with confocal, atomic force and near field microscopy, Biophys. J. 75 (1998) 342–353.
[30] A. Cruz, L. Vazquez, M. Velez, J. Perez-Gil, Influence of a fluorescent probe on the nanostructure of phospholipid membranes: dipalmitoylphosphatidylcholine interfacial monolayers, Langmuir 21 (2005) 5349–5355.
[31] A. Cruz, L. Vazquez, M. Velez, J. Perez-Gil, Effect of pulmonary surfactant protein SP-B on the micro- and nanostructure of phospholipid films, Biophys. J. 86 (2004) 308–320.
[32] V.M. Kaganer, H. Mohwald, P.K. Dutta, Structure and phase transitions in Langmuir monolayers, Rev. Mod. Phys. 71 (1999) 779–819.
[33] R.R. Harbottle, K. Nag, N.S. McIntyre, F. Possmayer, N.O. Petersen, Molecular organization revealed by time-of-flight secondary ion mass spectrometry of a clinically used extracted pulmonary surfactant, Langmuir 19 (2003) 3698–3704.
[34] M. Saleem, H.J. Galla, Surface view of the lateral organization of lipids and proteins in lung surfactant model systems—a ToF-SIMS approach, Biochim. Biophys. Acta 1798 (2009) 730–740.
[35] E. Keating, A.J. Waring, F.J. Walther, F. Possmayer, R.A. Veldhuizen, N.O. Petersen, A ToF-SIMS study of the lateral organization of lipids and proteins in pulmonary surfactant systems, Biochim. Biophys. Acta 1808 (2011) 614–621.
[36] S. Leporatti, G. Brezesinski, H. Mohwald, Coexistence of phases in monolayers of branched-chain phospholipids investigated by scanning force microscopy, Colloids Surf. Physicochemical Eng. Aspects 161 (2000) 159–171.
[37] C. Alonso, T. Alig, J. Yoon, F. Bringezu, H. Warriner, J.A. Zasadzinski, More than a monolayer: relating lung surfactant structure and mechanics to composition, Biophys. J. 87 (2004) 4188–4202.
[38] C.D. Blanchette, C.A. Orme, T.V. Ratto, M.L. Longo, Quantifying growth of symmetric and asymmetric lipid bilayer domains, Langmuir 24 (2008) 1219–1224.
[39] H.M. McConnell, Structures and transitions in lipid monolayers at the air–water interface, Annu. Rev. Phys. Chem. 42 (1991) 171–195.
[40] J. Bernardino de la Serna, J. Perez-Gil, A.C. Simonsen, L.A. Bagatolli, Cholesterol rules: direct observation of the coexistence of two fluid phases in native pulmonary surfactant membranes at physiological temperatures, J. Biol. Chem. 279 (2004) 40715–40722.
[41] J. Perez-Gil, Structure of pulmonary surfactant membranes and films: the role of proteins and lipid–protein interactions, Biochim. Biophys. Acta 1778 (2008) 1676–1695.
[42] O.G. Mouritsen, M.J. Zuckermann, What's so special about cholesterol? Lipids 39 (2004) 1101–1113.
[43] S.L. Veatch, S.L. Keller, Seeing spots: complex phase behavior in simple membranes, Biochim. Biophys. Acta 1746 (2005) 172–185.
[44] F. Possmayer, X. Jiao, L. Zhao, E. Keating, R.A. Veldhuizen, N.O. Petersen, Y.Y. Zuo, Comparative studies on bovine and rat pulmonary surfactants using AFM, Biophys. J. 96 (2009) 352a.
[45] Z. Leonenko, M. Rodenstein, J. Dohner, L.M. Eng, M. Amrein, Electrical surface potential of pulmonary surfactant, Langmuir 22 (2006) 10135–10139.
[46] Z. Leonenko, S. Gill, S. Baoukina, L. Monticelli, J. Doehner, L. Gunasekara, F. Felderer, M. Rodenstein, L.M. Eng, M. Amrein, An elevated level of cholesterol impairs self-assembly of pulmonary surfactant into a functional film, Biophys. J. 93 (2007) 674–683.
[47] M. Amrein, A. von Nahmen, M. Sieber, A scanning force- and fluorescence light microscopy study of the structure and function of a model pulmonary surfactant, Eur. Biophys. J. 26 (1997) 349–357.
[48] R.V. Diemel, M.M. Snel, L.M. Van Golde, G. Putz, H.P. Haagsman, J.J. Batenburg, Effects of cholesterol on surface activity and surface topography of spread surfactant films, Biochemistry 41 (2002) 15007–15016.
[49] R.V. Diemel, M.M. Snel, A.J. Waring, F.J. Walther, L.M. van Golde, G. Putz, H.P. Haagsman, J.J. Batenburg, Multilayer formation upon compression of surfactant monolayers depends on protein concentration as well as lipid composition. An atomic force microscopy study, J. Biol. Chem. 277 (2002) 21179–21188.
[50] S. Malcharek, A. Hinz, L. Hilterhaus, H.J. Galla, Multilayer structures in lipid monolayer films containing surfactant protein C: effects of cholesterol and POPE, Biophys. J. 88 (2005) 2638–2649.
[51] F. Hane, E. Drolle, Z. Leonenko, Effect of cholesterol and amyloid-beta peptide on structure and function of mixed-lipid films and pulmonary surfactant BLES: an atomic force microscopy study, Nanomedicine 6 (2010) 808–814.
[52] F. Hane, B. Moores, M. Amrein, Z. Leonenko, Effect of SP-C on surface potential distribution in pulmonary surfactant: atomic force microscopy and Kelvin probe force microscopy study, Ultramicroscopy 109 (2009) 968–973.
[53] J.A. Zasadzinski, J. Ding, H.E. Warriner, F. Bringezu, A.J. Waring, The physics and physiology of lung surfactants, Curr. Opin. Colloid Interface Sci. 6 (2001) 506–513.
[54] B. Piknova, V. Schram, S.B. Hall, Pulmonary surfactant: phase behavior and function, Curr. Opin. Struct. Biol. 12 (2002) 487–494.
[55] S. Rugonyi, S.C. Biswas, S.B. Hall, The biophysical function of pulmonary surfactant, Respir. Physiol. Neurobiol. 163 (2008) 244–255.
[56] J. Ding, D.Y. Takamoto, A. von Nahmen, M.M. Lipp, K.Y. Lee, A.J. Waring, J.A. Zasadzinski, Effects of lung surfactant proteins, SP-B and SP-C, and palmitic acid on monolayer stability, Biophys. J. 80 (2001) 2262–2272.
[57] K. Nag, J.G. Munro, K. Inchley, S. Schurch, N.O. Petersen, F. Possmayer, SP-B refining of pulmonary surfactant phospholipid films, Am. J. Physiol. 277 (1999) L1179–L1189.
[58] F. Possmayer, K. Nag, K. Rodriguez, R. Qanbar, S. Schurch, Surface activity in vitro: role of surfactant proteins, Comp. Biochem. Physiol. A Mol. Integr. Physiol. 129 (2001) 209–220.
[59] D. Schurch, O.L. Ospina, A. Cruz, J. Perez-Gil, Combined and independent action of proteins SP-B and SP-C in the surface behavior and mechanical stability of pulmonary surfactant films, Biophys. J. 99 (2010) 3290–3299.
[60] F. Baumgart, O.L. Ospina, I. Mingarro, I. Rodriguez-Crespo, J. Perez-Gil, Palmitoylation of pulmonary surfactant protein SP-C is critical for its functional cooperation with SP-B to sustain compression/expansion dynamics in cholesterol-containing surfactant films, Biophys. J. 99 (2010) 3234–3243.

[61] L. Gomez-Gil, J. Perez-Gil, E. Goormaghtigh, Cholesterol modulates the exposure and orientation of pulmonary surfactant protein SP-C in model surfactant membranes, Biochim. Biophys. Acta (2009) 1907–1915.
[62] S. Schurch, J. Goerke, J.A. Clements, Direct determination of volume- and time-dependence of alveolar surface tension in excised lungs, Proc. Natl Acad. Sci. U.S.A. 75 (1978) 3417–3421.
[63] M. Griese, Pulmonary surfactant in health and human lung diseases: state of the art, Eur. Respir. J. 13 (1999) 1455–1476.
[64] E. Keating, L. Rahman, J. Francis, A. Petersen, F. Possmayer, R. Veldhuizen, N.O. Petersen, Effect of cholesterol on the biophysical and physiological properties of a clinical pulmonary surfactant, Biophys. J. 93 (2007) 1391–1401.
[65] J.H. Ipsen, G. Karlstrom, O.G. Mouritsen, H. Wennerstrom, M.J. Zuckermann, Phase equilibria in the phosphatidylcholine-cholesterol system, Biochim. Biophys. Acta 905 (1987) 162–172.
[66] B.M. Discher, K.M. Maloney, D.W. Grainger, C.A. Sousa, S.B. Hall, Neutral lipids induce critical behavior in interfacial monolayers of pulmonary surfactant, Biochemistry 38 (1999) 374–383.
[67] K.Y. Lee, Collapse mechanisms of Langmuir monolayers, Annu. Rev. Phys. Chem. 59 (2008) 771–791.
[68] A. Gopal, V.A. Belyi, H. Diamant, T.A. Witten, K.Y.C. Lee, Microscopic folds and macroscopic jerks in compressed lipid monolayers, J. Phys. Chem. B 110 (2006) 10220–10223.
[69] C.Y. Tang, H.C. Allen, Ionic binding of Na + versus K + to the carboxylic acid headgroup of palmitic acid monolayers studied by vibrational sum frequency generation spectroscopy, J. Phys. Chem. A 113 (2009) 7383–7393.
[70] L. Pocivavsek, S.L. Frey, K. Krishan, K. Gavrilov, P. Ruchala, A.J. Waring, F.J. Walther, M. Dennin, T.A. Witten, K.Y. Lee, Lateral stress relaxation and collapse in lipid monolayers, Soft Matter 4 (2008) 2019–2029.
[71] S. Baoukina, L. Monticelli, H.J. Risselada, S.J. Marrink, D.P. Tieleman, The molecular mechanism of lipid monolayer collapse, Proc. Natl Acad. Sci. U.S.A. 105 (2008) 10803–10808.
[72] C. Laing, S. Baoukina, D.P. Tieleman, Molecular dynamics study of the effect of cholesterol on the properties of lipid monolayers at low surface tensions, Phys. Chem. Chem. Phys. 11 (2009) 1916–1922.
[73] N.N. Finer, Surfactant use for neonatal lung injury: beyond respiratory distress syndrome, Paediatr. Respir. Rev. 5 (Suppl A) (2004) S289–S297.
[74] E. Chong, J. Greenspan, S. Kirkby, J. Culhane, K. Dysart, Changing use of surfactant over 6 years and its relationship to chronic lung disease, Pediatrics 122 (2008) e917–e921.
[75] J. Hohlfeld, H. Fabel, H. Hamm, The role of pulmonary surfactant in obstructive airways disease, Eur. Respir. J. 10 (1997) 482–491.
[76] G. Enhorning, Surfactant in airway disease, Chest 133 (2008) 975–980.
[77] P.A. Dargaville, J.F. Mills, Surfactant therapy for meconium aspiration syndrome: current status, Drugs 65 (2005) 2569–2591.
[78] J.F. Lewis, R. Veldhuizen, The role of exogenous surfactant in the treatment of acute lung injury, Annu. Rev. Physiol. 65 (2003) 613–642.
[79] J.V. Been, L.J. Zimmermann, What's new in surfactant? A clinical view on recent developments in neonatology and paediatrics, Eur. J. Pediatr. 166 (2007) 889–899.
[80] D.G. Sweet, H.L. Halliday, The use of surfactants in 2009, Arch. Dis. Child. Educ. Pract. Ed. 94 (2009) 78–83.
[81] T.F. Yeh, H.C. Lin, C.H. Chang, T.S. Wu, B.H. Su, T.C. Li, S. Pyati, C.H. Tsai, Early intratracheal instillation of budesonide using surfactant as a vehicle to prevent chronic lung disease in preterm infants: a pilot study, Pediatrics 121 (2008) e1310–e1318.
[82] C.J. Lang, A.D. Postle, S. Orgeig, F. Possmayer, W. Bernhard, A.K. Panda, K.D. Jurgens, W.K. Milsom, K. Nag, C.B. Daniels, Dipalmitoylphosphatidylcholine is not the major surfactant phospholipid species in all mammals, Am. J. Physiol. Regul. Integr. Comp. Physiol. 289 (2005) R1426–R1439.
[83] B.A. Holm, Z. Wang, E.A. Egan, R.H. Notter, Content of dipalmitoyl phosphatidylcholine in lung surfactant: ramifications for surface activity, Pediatr. Res. 39 (1996) 805–811.
[84] Z. Leonenko, E. Finot, V. Vassiliev, M. Amrein, Effect of cholesterol on the physical properties of pulmonary surfactant films: atomic force measurements study, Ultramicroscopy 106 (2006) 687–694.
[85] L. Gunasekara, S. Schurch, W.M. Schoel, K. Nag, Z. Leonenko, M. Haufs, M. Amrein, Pulmonary surfactant function is abolished by an elevated proportion of cholesterol, Biochim. Biophys. Acta 1737 (2005) 27–35.
[86] R. Schmidt, P. Markart, C. Ruppert, M. Wygrecka, T. Kuchenbuch, D. Walmrath, W. Seeger, A. Guenther, Time-dependent changes in pulmonary surfactant function and composition in acute respiratory distress syndrome due to pneumonia or aspiration, Respir. Res. 8 (2007) 55.
[87] P. Markart, C. Ruppert, M. Wygrecka, T. Colaris, B. Dahal, D. Walmrath, H. Harbach, J. Wilhelm, W. Seeger, R. Schmidt, A. Guenther, Patients with ARDS show improvement but not normalisation of alveolar surface activity with surfactant treatment: putative role of neutral lipids, Thorax 62 (2007) 588–594.